Surface core-level shift and electronic structure on transition-metal diboride (0001) surfaces

Takashi Aizawa,* Shigeru Suehara, Shunichi Hishita, and Shigeki Otani
Advanced Materials Laboratory, National Institute for Materials Science, 1-1 Namiki, Tsukuba, Ibaraki 305-0044, Japan

Masao Arai
Computational Materials Science Center, National Institute for Materials Science, 1-1 Namiki, Tsukuba, Ibaraki 305-0044, Japan
(Received 6 August 2004; revised manuscript received 6 December 2004; published 6 April 2005)

Core levels of $NbB_2(0001)$ and $ZrB_2(0001)$ surfaces were measured by x-ray photoelectron spectroscopy (XPS). Large surface core-level shift (SCLS) to 1.6-eV shallower binding energy is observed in the B 1*s* core of the boron terminated $NbB_2(0001)$. By an *ab initio* density functional theory calculation, this SCLS is well reproduced. The analysis shows that the SCLS reflects not the total charge of the atom but the local charge density in the vicinity of the nucleus. The conventional XPS interpretation is not available in such a system with large intra-atomic charge redistribution. The electronic structure which leads the charge redistribution is discussed.

DOI: 10.1103/PhysRevB.71.165405 PACS number(s): 79.60.Bm, 73.20.At, 71.20.Ps

I. INTRODUCTION

On various surfaces, core levels measured by x-ray photoelectron spectroscopy (XPS) appear at different energy from that in the bulk, which is known as a surface core-level shift (SCLS). The SCLSs are usually in a fraction of eV on elemental metal surfaces because of the two canceling effects:[1] One is the "environmental" effect, in which the spreading electrons from surrounding atoms increase the shielding of the nucleus potential to decrease the binding energy. The other is the "hybridization" effect, in which the electron promotion from a compact orbital to a larger one to make bonds to surrounding atoms decreases the shielding and increases the binding energy. If these two effects are comparable, creating a surface spontaneously reduces these effects to make the small SCLS.

On compounds' surfaces having more ionicity, larger SCLSs are reported but the interpretation is restricted in the conventional XPS framework: difference in the charged state at the surface. For example, −1.3 eV SCLSs are reported on a pyrite (FeS_2) surface,[2] which are assigned to a monosulfide species S^{2-} formed on the surface by breaking a S_2^{2-} bond. The hybridization effect is not fully understood in such a compound.

A transition-metal diboride (MB_2) has unique features of high hardness, high melting point, and metallic (or semimetallic) conductivity. It has been used as a thin film resistor, a diffusion barrier layer in micro devices, hard coating, and so on. It is also expected to be used as a new material for a cold electron emitter, a catalyst, or a substrate for GaN film deposition.[3–6] These features originate from the unique bonds having covalent, metallic, and ionic characters together. It crystallizes in an AlB_2-type crystal structure, which consists of alternate stacking of a graphitelike boron layer and a close-packed metal layer. Within the boron layer, there are strong covalent bonds between boron atoms. Between metal atoms metallic bonds exist. Between metal and boron, not only ionic but also covalent bonds are suggested. For better understanding of SCLS, it is worthwhile to investigate such a unique bonding system.

The $MB_2(0001)$ surface is terminated by either the metal layer or the boron layer, namely a polar surface. The surface termination is different between group 4 (Zr, Hf) $MB_2(0001)$ and group 5 (Nb, Ta) $MB_2(0001)$. By ion scattering spectroscopy, clean (0001) surfaces of HfB_2 and TaB_2 are revealed to be terminated with the metal layer[7] and the boron layer,[8] respectively. The high-resolution electron energy loss spectroscopy (HREELS) experiment has supported the metal and boron termination of $ZrB_2(0001)$ and $NbB_2(0001)$, respectively.[9] First-principles total energy calculation[10] showed that excess electrons in the TaB_2 compared with the HfB_2 stabilize the surface boron layer. The $MB_2(0001)$ surface can be a prototype for polar surfaces because both polarities are available on almost the same crystal structure. Recently, the chemical reactivity between $HfB_2(0001)$ and $TaB_2(0001)$ was revealed to be different, reflecting the surface termination.[11,12]

On the metal-terminated surfaces such as $HfB_2(0001)$ (Ref. 13) or $ZrB_2(0001)$ (Refs. 14 and 15), XPS shows no SCLS on the B 1*s* level. On the other hand, Evstigneeva *et al.*[12] reported recently the shift of the surface B 1*s* level toward ~1.5-eV shallower binding energy than the bulk on $TaB_2(0001)$. They discussed this SCLS but did not reach a conclusion about chemical status of the surface boron layer. In this paper, the XPS results of the boron-terminated $NbB_2(0001)$ and the metal-terminated $ZrB_2(0001)$ are presented and the B 1*s* SCLS of −1.6 eV is reported in the former. This SCLS is much larger than those on elemental metals, and rather comparable to those for a ionic compounds. However, this large SCLS cannot be explained by the conventional ionic or charge transfer model. The mechanism of the SCLS is investigated by means of the first-principles total-electron calculations based on the density functional theory (DFT). We found that a significant electron redistribution in the surface B atom, namely the hybridization effect, induces the large SCLS in this system.

II. EXPERIMENT

The measurements were made by using a conventional XPS system (VG ESCALAB 200) combined with ultrahigh

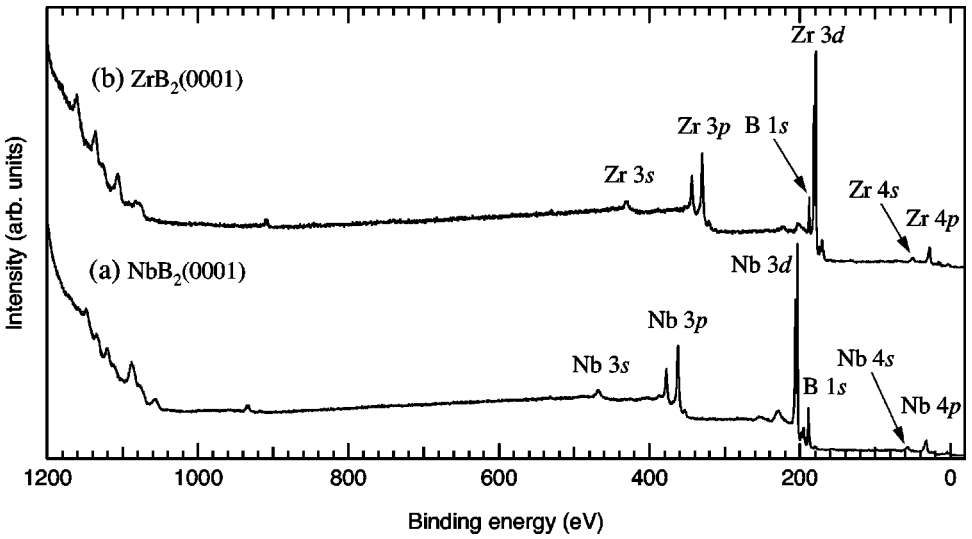

FIG. 1. Wide-range XPS spectra for clean (a) NbB_2(0001) and (b) ZrB_2(0001) surfaces with use of Mg $K\alpha$ source ($\hbar\omega$=1253.6 eV). The binding energy is measured from the Fermi energy.

vacuum (UHV) sample preparation and transfer chambers. The base pressure of the spectrometer was less than 2×10^{-8}Pa. The spectrometer has a dual (Mg and Al) anode x-ray source and a monochromated Al source. The photoelectron energy is analyzed by a spherical-sector electrostatic energy analyzer. The energy scale was calibrated with the Ag $3d_{5/2}$ peak (368.2 eV) for a sputter-cleaned Ag sample. The energy resolution was ~0.86 eV in the full width at half maximum (FWHM) with the monochromated x-ray source.

The preparation chamber was equipped with an ion gun for Ar^+-ion bombardment and a low-energy electron diffraction (LEED) optics to check the surface ordering. The sample can be heated by electron bombardment from the backside, and the temperature was measured by an optical pyrometer. The prepared sample was carried to the spectrometer in the UHV of 10^{-8} Pa range. The final flash heating was done in the spectrometer chamber just before every measurement.

The single crystals used in this experiment were grown by the rf-heated floating-zone method in our laboratory.[16–18] They were oriented by x-ray Laue method within 1 deg from the ⟨0001⟩ axis, and were sliced by a spark-erosion cutter in disks (~8 mm in diameter and ~1 mm in thickness). One side of the sample was mechanically polished to a mirror finish with diamond (9 and 3 μm) and alumina (1 μm) powder. The sample surfaces were prepared by procedures similar to those described in the literature.[9] Briefly, the ZrB_2(0001) was cleaned by several cycles of flash heating at 2200 K in the UHV after degas heating at 1400 K. The NbB_2(0001) was cleaned by several Ar^+-ion bombardment (5 keV, 10 μA, 20 min) and 1500 K annealing cycles. The clean surfaces showed sharp 1×1 LEED patterns, and little contamination was detected in the XPS measurement.

The obtained XPS spectra were analyzed as follows. Around the B 1*s* peak, the background is subtracted. The background is estimated by Shirley's method[19,20] on the NbB_2 spectra. On the ZrB_2 spectra, the background is assumed to be a linear function because Shirley's method is unavailable due to a large tail of the Zr 3*d* peak. After the background subtraction, the peak is fitted to a Voigt-type function.

III. EXPERIMENTAL RESULTS

Figure 1 shows wide-range XPS spectra acquired with a Mg $K\alpha$ source. On both spectra for NbB_2(0001) and ZrB_2(0001), little contamination of O or C is detected. The observed binding energies measured from Fermi level are summarized in Table I. A small peak at ~935 eV and at ~910 eV in Fig. 1(a) and Fig. 1(b), respectively, is attributed to ghost peaks of M 3*d* caused by an O $K\alpha$ line from oxygen contamination on the x-ray source anode.

Figure 2 shows the B 1*s* region. Solid circles are normalized and background-subtracted data points measured by using the monochromated Al $K\alpha$ source. The spectra 2(a) and 2(b) were acquired on the NbB_2(0001) sample with detection angles of 0° and 60° from the surface normal, respectively.

TABLE I. Observed core-level binding energies from Fermi level in eV.

Core	NbB_2(0001)	ZrB_2(0001)
B 1*s* (bulk)	188.7	187.9
B 1*s* (surface)	187.1	···
B 1*s* (defect)	187.8	···
M $4p_{3/2}$	32.1	27.5
M $4p_{1/2}$	34.3	29.2
M 4*s*	57.3	50.3
M $3d_{5/2}$	203.6	178.9
M $3d_{3/2}$	206.3	181.3
M $3p_{3/2}$	362.1	329.9
M $3p_{1/2}$	377.6	343.5
M 3*s*	467.9	430.1

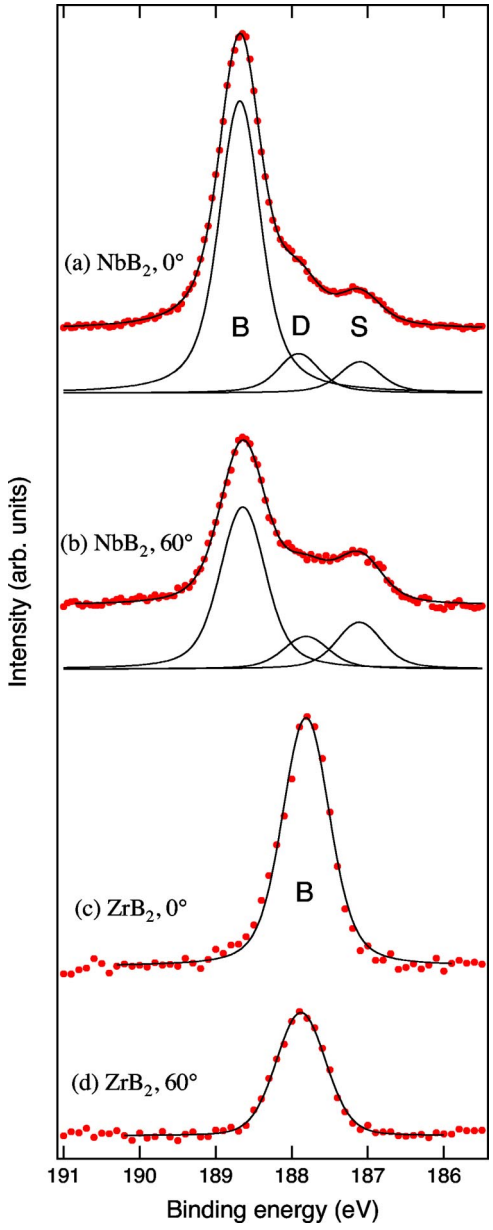

FIG. 2. (Color online) B 1*s* XPS peak of $NbB_2(0001)$ [(a) and (b)] and $ZrB_2(0001)$ [(c) and (d)]. The detection angle for (a) and (c) is 0°, and for (b) and (d) is 60° from the surface normal, respectively. The x-ray source is monochromated Al $K\alpha$ ($\hbar\omega$=1486.6 eV). The binding energy is measured from the Fermi level. After being normalized by the background intensity, the background has been subtracted. Solid circles are measured data and curves are the fitted Voigt function. On $NbB_2(0001)$, three peaks *B*, *S*, and *D* are found correspond to bulk, surface, and defect components, respectively. On $ZrB_2(0001)$, only the bulk (*B*) component is observed.

The spectra 2(c) and 2(d) are those for $ZrB_2(0001)$. After being normalized by the background intensity, the background has been subtracted. The spectra are fitted to a Voigt-type function, in which a few Lorentzian peaks are convoluted with a Gaussian function. The fitting results are shown in Fig. 2 by solid curves.

TABLE II. Calculated bulk lattice parameters and interlayer distances d_{ij} between the layers *i* and *j* in the slab configuration. In the parentheses are their deviation from the bulk values. Layer 1 denotes the surface layer. Experimental (Expt.) values are listed for comparison.

	NbB_2	ZrB_2
a (pm)	311.0	316.9
Expt.[a]	310.9	316.9
$c/2$ (pm)	166.5	177.6
Expt.[b]	164.4	176.5
d_{12} (pm)	166.6 (+0.07%)	169.6 (−4.47%)
d_{23} (pm)	165.2 (−0.76%)	178.3 (+0.43%)
d_{34} (pm)	166.8 (+0.18%)	177.7 (+0.07%)
d_{45} (pm)	166.6 (+0.09%)	177.8 (+0.13%)
d_{56} (pm)	166.7 (+0.14%)	177.5 (−0.02%)
d_{67} (pm)	166.4 (−0.03%)	177.5 (−0.03%)

[a]Reference 18.
[b]Reference 17.

The NbB_2 spectra, Fig. 2(a) and Fig. 2(b), are well reproduced with three peaks. A main peak *B* appears at 188.7 eV, and subpeaks *S* and *D* at 187.1 and 187.8 eV, respectively. The peak-*B* intensity decreases with the detection angle, while the peak-*S* grows relatively. This fact shows that peak *B* is attributed to the boron in the bulk, and peak *S* to the outermost boron layer, respectively. The angle dependency of peak *D* is not as clear. The calculation described in the following sections suggests that the origin of peak *D* is in some defect structures.

On the other hand, the ZrB_2 spectra are satisfactorily fitted by a single peak as seen in Fig. 2(c) and Fig. 2(d). In this case, no SCLS is observed either in the B 1*s* level or in the Zr 3*d* levels (not shown) within the experimental resolution. All observed peak positions (Table I) correspond well to those reported in the literature.[14]

From the experimental fact, it is clear that the boron atoms in the surface layer have smaller 1*s* binding energy than in the bulk. In the following sections we will show the *ab initio* calculations, giving a clear explanation of the SCLS.

IV. CALCULATION

First-principles calculations were performed by using the WIEN2k code,[21] which is based on the full-potential method using the augmented-plane-wave plus local orbitals (APW+lo) basis[22,23] within the DFT. In this work, exchange interactions and correlation effects are treated with the generalized gradient approximation (GGA) of Perdew *et al.*[24] The calculations were performed on a workstation (Dell Precision 450: two Xeon 3 GHz CPUs) and a calculation server at NIMS (Hitachi SR11000).

At first, the bulk lattice parameter was optimized. The convergence was checked for the muffin-tin radius and a number of sampling points (*k* points) in the Brillouin zone. Minimum muffin-tin radius R_{MT} and cutoff wave number for

TABLE III. Calculated boron 1*s* and metal $3d_{5/2}$ core-level energies from Fermi level in eV. GS and TS denote the ground-state and transition-state calculations, respectively. In the GS calculations, the energy is measured from the Fermi energy. Rx and NoRx mean whether the surface is relaxed or not. For comparison, experimental binding energies are listed in the Expt. column. B1 denotes the outermost boron layer and Nb2 the second outermost niobium layer, and so on.

NbB_2	GS (NoRx)	GS (Rx)	TS	Expt.
B1	172.76	172.75	184.88	187.1
B3	174.16	174.17		
B5	174.33	174.32	186.73	
B7	174.29	174.29		
B(bulk)	174.32			188.7
SCLS	−1.57	−1.57	−1.85	−1.6
Nb2	192.25	192.23		
Nb4	192.51	192.51		
Nb6	192.43	192.43		
Nb(bulk)	192.50			203.6
ZrB_2				
B2	173.32	173.29	185.61	
B4	173.34	173.32		
B6	173.37	173.36	185.81	
B(bulk)	173.53			187.9
Zr1	167.92	167.79		
Zr3	167.38	167.35		
Zr5	167.43	167.43		
Zr7	167.43	167.43		
Zr(bulk)	167.61			179.0

the basis set K_{max} were selected as $R_{MT}K_{max}=6.0$. The muffin-tin radii of boron and metal were taken to be 1.4 and 2.4 a.u., respectively. This condition corresponds to the cutoff energy of 18.4 Ry. For the bulk calculation $(10\times10\times8)$ *k* points were accumulated. The optimized lattice parameters of the bulk are listed in Table II.

In order to examine the surface effects, a supercell structure is adopted along the *c* axis. The convergence for the slab and vacuum thickness was checked, resulting in the unit cell of 13 atomic layers (7 B+6 Nb layers for NbB_2, and 7 Zr+6 B layers for ZrB_2) separated by a vacuum layer 20 a.u. thick. As no sign of reconstruction is found in the experiments (1×1) periodicity is taken along the surface in the ground-state calculations and $(8\times8\times1)$ *k* points were sampled for the total-energy calculation. As the surface may have some relaxation, the interlayer distances were varied according to the residual forces until they decreased to less than 2 mRy/a.u. The obtained lattice spacing is shown in Table II. It should be noted that the relaxation for $NbB_2(0001)$ is not as large as suggested by the ion-scattering experiment on $TaB_2(0001)$.[8] On the contrary, the surface relaxation on $ZrB_2(0001)$ is considerable.

TABLE IV. Calculated total electron number in the muffin-tin sphere (q_{tot}) and the charge density at the nucleus [$(\rho(0)$] in atomic units. Val means the density of valence electrons and Tot means the total (valence + core) electron density. Layer notation such as B1 is in the same manner as in Table III.

NbB_2	q_{tot}	$\rho(0)$(Val)	$\rho(0)$(Tot)
B1	3.060	2.139	72.060
B3	3.121	2.028	71.941
B5	3.117	2.014	71.930
B7	3.118	2.012	71.928
B(bulk)	3.118	2.018	71.933
Nb2	38.773	234.96	81182.65
Nb4	38.823	234.02	81182.76
Nb6	38.832	233.91	81181.66
Nb(bulk)	38.833	234.05	81181.82
ZrB_2			
B2	3.097	2.040	71.959
B4	3.095	2.040	71.960
B6	3.094	2.039	71.959
B(bulk)	3.089	2.038	71.959
Zr1	37.559	200.67	73502.81
Zr3	37.661	199.26	73501.23
Zr5	37.652	199.24	73501.22
Zr7	37.649	199.23	73501.21
Zr(bulk)	37.632	199.27	73501.24

By the ground-state calculation, the energy difference before the photoemission process, namely the initial-state effect, is clarified. However, the electron relaxation effect after the photoemission process, the final-state effect, also may vary between the surface and in the bulk. In order to check the final-state effect, the Slater-Janak transition-state calculation[25,26] was performed for the B 1*s* state. In the transition-state calculation, the supercell was expanded to (2×2) along the surface in order to avoid neighboring ionized atoms. Accordingly, the *k* points were reduced to $(4\times4\times1)$. Half of an electron is picked off from the B 1*s* orbital in the surface B or in the subsurface B to simulate the binding energy. In order to keep the charge neutrality, the same amount of charge is donated back to the conduction band.

V. CALCULATION RESULTS AND DISCUSSIONS

A. Binding energy

The calculated energies for boron 1*s* and metal 3*d* are listed in Table III. The *ab initio* calculation correctly reproduces the SCLS of the B 1*s* on $NbB_2(0001)$ already in the ground-state (GS) calculation. The SCLS is a little overestimated by the transition-state (TS) calculation, but the abso-

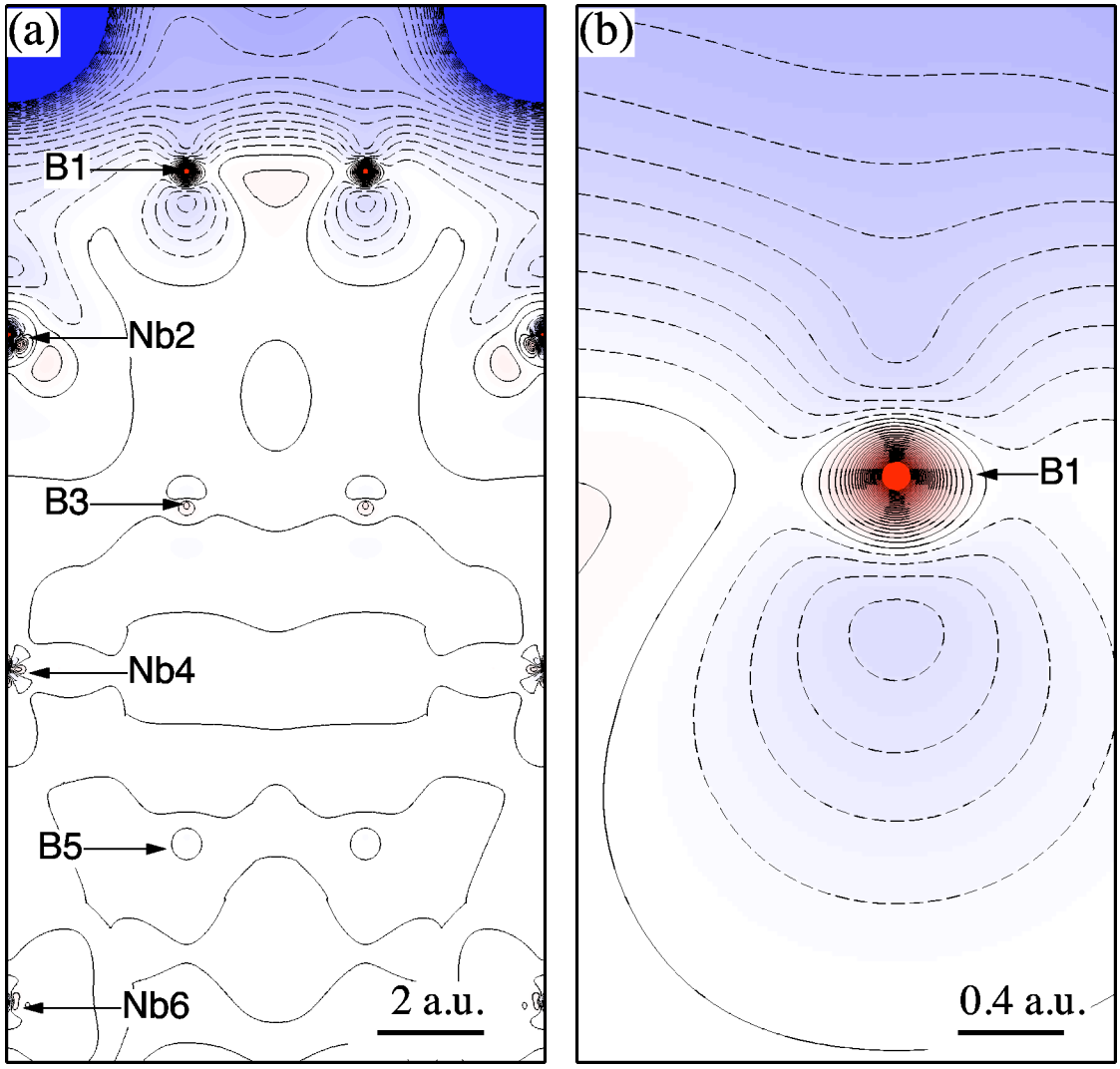

FIG. 3. (Color) (a) $(11\bar{2}0)$ sectional map of electron-density difference between $NbB_2(0001)$ surface and bulk, and (b) its close-up (5×) around the surface boron. The bulk electron density is subtracted from the nonrelaxed slab one. The notations B*i* and Nb*i* are the same as in Table III. Solid and dashed curves are positive and negative contours, respectively.

lute value of the binding energy better approaches the experiment. As the main feature of the observed SCLS appears already in the initial state, the final-state effect seems unimportant in the SCLS here. As shown in Table II, the surface relaxation is small on $NbB_2(0001)$, resulting in the small differences in the GS energies between the relaxed model and the nonrelaxed model. The SCLS is caused not by the lattice-relaxation effect but by the truncation of the bond itself. As for Nb 3*d* levels, little difference is calculated layer by layer, which reproduces the experiment well. The calculated core-level shift as small as 0.2 eV is in the similar range observed in pure metal surfaces.[1]

In the ideal boron-terminated model, only two components appear for B 1*s* corresponding to peak *B* and peak *S* in the experiment. The other observed peak, *D*, is not reproduced. In order to investigate the origin of the peak *D*, preliminary calculations were done for the two structures modeled on presumable defects at the surface: One is Nb adatom and the other is B vacancy. In these calculations, the atomic structure was not optimized. For the Nb adatom model, one Nb adatom is introduced in each 2×2 unit cell at the same site as in the bulk, which causes the B 1*s* core-level shift of −1.1 eV beneath the adatom. For the B vacancy model, one B atom is picked off from each $\sqrt{3}\times\sqrt{3}$ unit cell, leaving the others fixed at the same position. In this model, the SCLS of −0.8 eV was calculated at the neighboring B site to the vacancy. At the second nearest-neighbor site, the B 1*s* SCLS was estimated to be −1.6 eV, which is hardly affected by the vacancy. As these calculations do not consider lattice relaxation, the calculated value may not be accurate enough to judge which defect is the case. However, the *D* peak is reasonably attributed to such defect structures as Nb adatoms or B vacancies, or both.

In the case of $ZrB_2(0001)$ slab, little B 1*s* energy difference is found between the layers in both the GS and TS calculations, which is quite consistent with the experiment. The B 1*s* level for ZrB_2 lies between that of B at the surface and of B in bulk for NbB_2, which also agrees with the experiment. The GS calculation for the nonrelaxed model shows $\sim+0.5$ eV SCLS in the Zr 3*d* level. This SCLS is a

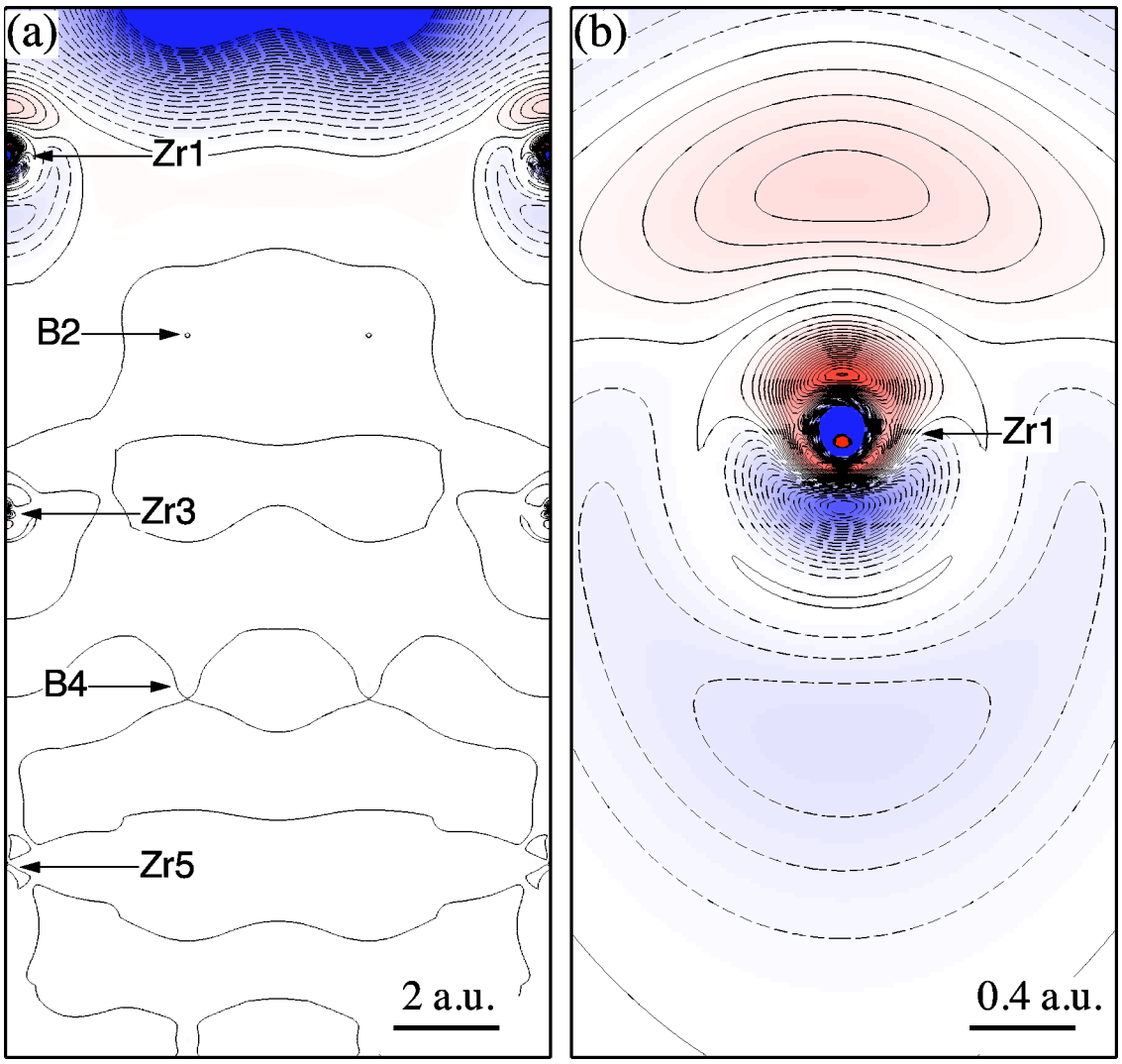

FIG. 4. (Color) (a) $(11\bar{2}0)$ sectional map of electron-density difference between $ZrB_2(0001)$ surface and bulk, and (b) its close-up (5 ×) around the surface Zr. The bulk electron density is subtracted from the nonrelaxed slab one. The notations Zr*i* and B*i* are the same as in Table III. Solid and dashed curves are positive and negative contours, respectively.

little reduced after the surface relaxation, which should not be resolved with the conventional XPS experiment. The effect of considerable surface relaxation is not large in the Zr 3*d* levels.

B. Charge distribution

Nowadays, most XPS core level measurements are done to find the charged state of the atom. What is indicated about the charged state of B by the SCLS? The total charge within the muffin-tin sphere (q_{tot}) and the charge density at the nucleus [$\rho(0)$] are listed in Table IV. While the q_{tot} of the surface B (B1) is decreased on $NbB_2(0001)$, the $\rho(0)$ is increased, on the contrary. This is mainly caused by the valence electrons as shown in Table IV. The 1*s* orbital is spatially so compact ($\langle r \rangle \sim 0.33$ a.u.) that it feels the shielding effect only near the nucleus. Therefore, the 1*s* level reflects the charge density near the nucleus rather than the total charge of the atom.

The opposite variation of the q_{tot} and the $\rho(0)$ indicates significant redistribution of the valence electrons at the surface. In Fig. 3, a difference map of the total electron density between the slab model and the bulk model is shown. The loss of Nb atoms at the surface is represented by steep holes near the upper corners in Fig. 3(a). In the interatomic region between B1 and the missing Nb, electron density which has been concerned with the bonding is reduced. Around the B1 atoms, the up- and down sides of the atom are especially depressed as shown in Fig. 3(b), which corresponds to the π ($2p_z$) orbital. This indicates that the π orbital mainly contributes to the B–Nb bonding. The electrons released from the interatomic bond condense in the region near the atom: maybe 2*s* orbital, and partly in the bond between the nearest-neighbor B1 atoms: $2p_x+2p_y$ orbitals. This redistribution causes the inconsistent appearance of the total-charge decrease and the increase near the nucleus.

In the case of $ZrB_2(0001)$, the charge distribution on the boron atoms hardly deviates from the bulk even at the second layer (B2), as shown in Table IV and in Fig. 4(a), be-

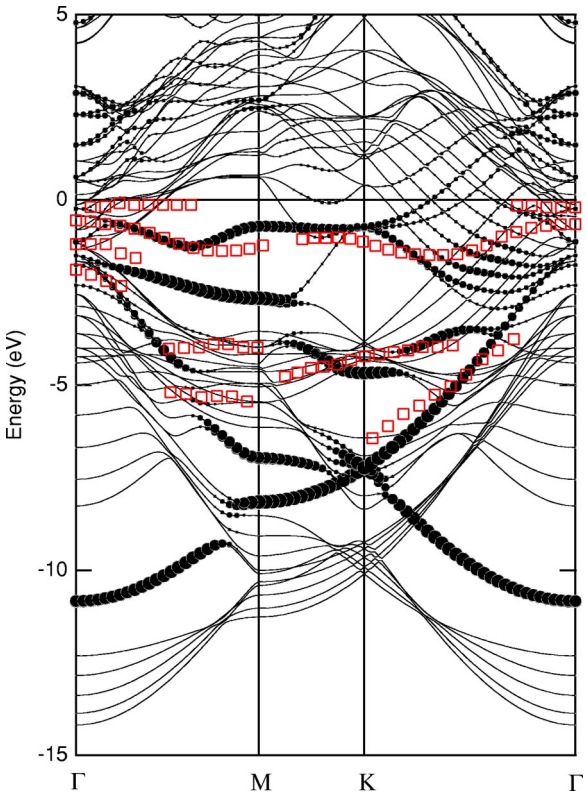

FIG. 5. Calculated electronic band dispersion for $NbB_2(0001)$ 13-layer slab. Solid circles' radii correspond to the contribution of the surface B atom. Open squares are the ARUPS data (Ref. 27) for $TaB_2(0001)$.

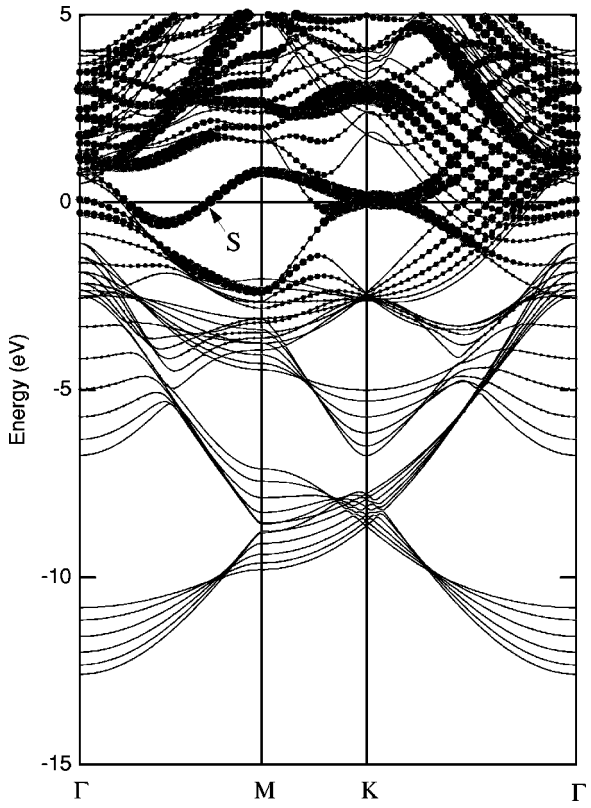

FIG. 6. Calculated electronic band dispersion for $ZrB_2(0001)$ 13-layer slab. Solid circles' sizes denote the first layer Zr contribution. A band labeled *S* is the surface band.

cause no nearest-neighbor B–Zr bond is missing. The B 1*s* SCLS does not appear there. In the Zr atoms, the outermost atom (Zr1) has larger $\rho(0)$ but smaller q_{tot}. Although this situation is the same as the B1 atom on $NbB_2(0001)$, the SCLS is not as large as in the NbB_2. The reason for the small Zr 3*d* SCLS is the following: As shown in Fig. 4, the charge density indeed increases as near to the nucleus as $r<0.02$ a.u., but decreases just around it (up side: $0.03<r<0.16$; down side: $0.02<r<0.06$), and then increases again (up side: $0.16<r$; down side: $0.06<r<0.13$). In the downward direction, it decreases again ($0.13<r$). Here, r is a distance from the Zr1 nucleus measured by a.u. This alternate deviation may be caused by interference between Zr 4*d*, 5*s*, and 5*p* orbitals, which are the valence bands most affected by the surface formation. Such alternate charge deviation must be integrated within the 3*d*-core region ($\langle r\rangle \sim 0.45$ a.u.). The resulting energy shift can be small. In the case of B1 on $NbB_2(0001)$, the charge density simply increases around the nucleus in the relatively large region of $r<0.22$ a.u., so that $\rho(0)$ can represent the charge variation that the B 1*s* electron feels.

C. Band dispersion

The calculated electronic band dispersion relations for the slab models are shown in Fig. 5 and Fig. 6. On $NbB_2(0001)$, distinct surface bands appear as marked by solid circles, the size of which indicates the B1 component. The surface band lying at ~ -1.0 eV along the $\Gamma-M$ and $M-K$ axis has B1 $2p_z$ character, namely the surface π band. The other surface bands having deeper energy have the σ character. Their shallower energy parts are contributed mainly by the B1 $2p_x+2p_y$ orbitals, and their deeper (<-6 eV) energy parts consist mainly of the 2*s* orbital. The surface band dispersion data[27] measured by angle-resolved ultraviolet photoelectron spectroscopy (ARUPS) on $TaB_2(0001)$ is plotted by open squares for the sake of comparison. The main peak observed in ARUPS is the surface π band, which is well reproduced by the calculation. Reasonable agreement is observed in the other σ bands as well.

The surface σ bands appear at lower binding energy than the corresponding bulk bands. As mentioned in Sec. V B, electrons transfer from the π band to the σ band at the surface B layer. The charge increment induces more electron-electron interaction to decrease the orbital's binding energy. The observed σ band energy is consistently explained by the charge acceptance in the 2*s* and $2p_x+2p_y$ orbitals. As for the surface π band, the corresponding bulk π band is not so clear because of the strong mixing with the Nb 4*d* orbitals. In fact, the calculation indicates that the surface π band is not distinctively resolved from the bulk band on the $\Gamma-K$ axis. As the π band is no longer rigid, it is difficult to discuss the charge donation effect alone.

In the $ZrB_2(0001)$ band, no surface band concerned with boron appears. One surface band (labeled "*S*" in Fig. 6) appears around the Fermi level and crosses it several times. The population analysis indicates that this surface band consists of complex hybridization of 4*d*, 5*s*, and 5*p* orbitals of the surface Zr atom. As this band is partially filled, the complex interferential charge redistribution might occur as discussed in Sec. V B. From this band structure, the $ZrB_2(0001)$ surface is suggested to have strong metallic character. This is consistent with the dissociative adsorption of some molecules[28] on this surface.

D. Comparison with the conventional framework

In a conventional XPS interpretation, the more positively (negatively) an atom is charged, the deeper (shallower) the core-level binding energy becomes because of the less- (more) screening effect of the nucleus charge. In the case of $NbB_2(0001)$, the surface B is less negative than the bulk B. This is consistent with the electron negativity: The Pauling's (Mulliken's) electronegativity of B is 2.0 (4.3 eV), which is larger than that of Nb: 1.6 (3.8 eV) or Zr: 1.4 (3.5 eV). B is expected to accept some electrons from the surrounding metal atoms. At the surface, the B atoms lose half of the neighboring Nb atoms, so that the negative charge should be reduced compared with the bulk B atoms. This might lead to the wrong prediction that the surface B has larger 1*s* binding energy in the conventional XPS interpretation.

The conventional XPS interpretation is true only if the charge redistribution within the atom is small, where the charge variation must be smoothly distributed so that q_{tot} and $\rho(0)$ should change similarly. In systems of strong covalency, where large intra-atomic redistribution (hybridization effect) is expected, the XPS core-level shift does not necessarily correspond to the charged state.

VI. SUMMARY

The large surface core-level shift was found on the B 1*s* level on the B-terminated $NbB_2(0001)$ surface. The core level was shifted to shallower binding energy at the surface. The *ab initio* DFT calculation clarifies that the core-level shift is determined not by the total charge of the atom but by the electron density in the vicinity of the nucleus. The large intra-atomic charge redistribution is found in the surface B atom. The truncation of the B–Nb bond at the surface causes charge redistribution from the missing bond to the surface atom, which explains the reduction of the charge and the shallower binding energy consistently. It is shown that the XPS chemical shift does not necessarily relate to the charged state in covalent compounds.

ACKNOWLEDGMENTS

We wish to express our many thanks to Dr. K. Kobayashi of NIMS for helpful discussions. We also acknowledge Dr. H. Kawanowa for providing previously published ARUPS data.

*aizawa.takashi@nims.go.jp

[1] P. S. Bagus, C. R. Brundle, G. Pacchioni, and F. Parmigiani, Surf. Sci. Rep. **19**, 265 (1993).
[2] H. W. Nesbitt, G. M. Bancroft, A. R. Pratt, and M. J. Scaini, Am. Mineral. **83**, 1067 (1998).
[3] H. Kinoshita, S. Otani, S. Kamiyama, H. Amano, I. Akasaki, J. Suda, and H. Matsunami, Jpn. J. Appl. Phys., Part 2 **40**, L1280 (2001).
[4] J. Suda and H. Matsunami, J. Cryst. Growth **237–239**, 1114 (2002).
[5] Y. Tomida, S. Nitta, S. Kamiyama, H. Amano, I. Akasaki, S. Otani, H. Kinoshita, R. Liu, A. Bell, and F. A. Ponce, Appl. Surf. Sci. **216**, 502 (2003).
[6] H. Kinoshita, S. Otani, S. Kamiyama, H. Amano, I. Akasaki, J. Suda, and H. Matsunami, Jpn. J. Appl. Phys., Part 1 **42**, 2260 (2003).
[7] W. Hayami, R. Souda, T. Aizawa, and T. Tanaka, Surf. Sci. **415**, 433 (1998).
[8] H. Kawanowa, R. Souda, S. Otani, and Y. Gotoh, Phys. Rev. Lett. **81**, 2264 (1998).
[9] T. Aizawa, W. Hayami, and S. Otani, Phys. Rev. B **65**, 024303 (2002).
[10] K. Yamamoto, K. Kobayashi, H. Kawanowa, and R. Souda, Phys. Rev. B **60**, 15 617 (1999).
[11] M. Belyansky and M. Trenary, Inorg. Chim. Acta **289**, 191 (1999).
[12] A. Evstigneeva, R. Singh, M. Trenary, and S. Otani, Surf. Sci. **542**, 221 (2003).
[13] C. L. Perkins, R. Singh, M. Trenary, T. Tanaka, and Y. Paderno, Surf. Sci. **470**, 215 (2001).
[14] R. Singh, M. Trenary, and Y. Paderno, Surf. Sci. Spectra **7**, 310 (2000).
[15] C. Jariwala, A. Chainani, S. Tsuda, T. Yokoya, S. Shin, Y. Takano, K. Togano, S. Otani, and H. Kito, Phys. Rev. B **68**, 174506 (2003).
[16] S. Otani and Y. Ishizawa, J. Cryst. Growth **165**, 319 (1996).
[17] S. Otani, M. M. Korsukova, and T. Mitsuhashi, J. Cryst. Growth **186**, 582 (1998).
[18] S. Otani, M. M. Korsukova, and T. Mitsuhashi, J. Cryst. Growth **194**, 430 (1998).
[19] D. A. Shirley, Phys. Rev. B **5**, 4709 (1972).
[20] *Practical Surface Analysis by Auger and X-ray Photoelectron Spectroscopy*, edited by D. Briggs and M. P. Seah (Wiley, New York, 1983), pp. 181–216.
[21] P. Blaha, K. Schwarz, G. K. H. Madsen, D. Kvasnicka, and J. Luitz, WIEN2K, *An Augmented Plane Wave + Local Orbitals Program for Calculating Crystal Properties* (Karlheintz Schwarz, Techn. Universität Wien, Vienna, Austria, 2001).
[22] E. Sjöstedt, L. Nordström, and D. J. Singh, Solid State Commun. **114**, 15 (2000).
[23] K. Schwarz, P. Blaha, and G. K. H. Madsen, Comput. Phys. Commun. **147**, 71 (2002).

[24] J. P. Perdew, J. A. Chevary, S. H. Vosko, K. A. Jackson, M. R. Pederson, D. J. Singh, and C. Fiolhais, Phys. Rev. B **46**, 6671 (1992).
[25] J. C. Slater, *Quantum Theory of Molecules and Solids* (McGraw-Hill, New York, 1974), Vol. 4, pp. 51–55.
[26] J. F. Janak, Phys. Rev. B **18**, 7165 (1978).
[27] H. Kawanowa, R. Souda, K. Yamamoto, S. Otani, and Y. Gotoh, Phys. Rev. B **60**, 2855 (1999).
[28] T. Aizawa, W. Hayami, and S. Otani, J. Chem. Phys. **117**, 11310 (2002).